PCCP

Accepted Manuscript

This article can be cited before page numbers have been issued, to do this please use: Y. Wang, K. Wu and D. Cubero, *Phys. Chem. Chem. Phys.*, 2019, DOI: 10.1039/C8CP06897F.

ROYAL SOCIETY OF CHEMISTRY

rsc.li/pccp

View Article Online
DOI: 10.1039/C8CP06897E

Journal Name

ARTICLE TYPE

Cite this: DOI: 10.1039/xxxxxxxxxx

An excess electron at polyethylene/vacuum interfaces using a reaction-field technique†

Yang Wang[a], Kai Wu[a] and David Cubero*[b]

Received Date
Accepted Date

DOI: 10.1039/xxxxxxxxxx

www.rsc.org/journalname

We study the surface states of an excess electron at polyethylene/vacuum interfaces using an accurate reaction-field method, specifically designed to take into account the long range interaction of the excess electron and the dielectric surface. The method is shown to validate the energy levels recently reported with a simple perturbation theory scheme, while providing a better description of the wave function at the vacuum. The use of a single particle pseudopotential allows the simulation of large interface samples, showing distinct differences between the electron surface states at amorphous and crystalline interfaces due to their different atomic density.

1 Introduction

The nature of the dynamics and trapping of excess electrons in condensed matter is of considerable interest due to its appearance in numerous applications, from photovoltaics[1] to electrical insulation[2] and the design of new nanocomposite dielectrics[3], to name a few.

The study of a single excess electron in an atomic environment also serves as a paradigm for mapping complex many-body problems, where electron correlation effects are important, into simpler one-electron models.

Our focus here is polyethylene (PE), the polymeric organic insulator with the simplest chemical structure (a polymer with a repeated monomer —CH_2—), with uncountable industrial applications, from kitchen boards to high-tension cables. Excess-electron trapping in polyethylene has been linked to aging and dielectric breakdown[2].

One-electron pseudopotential methods, using mixed quantum-classical simulations, have been shown to be the state of the art for the excess electron in simple fluids such as water[4–6], methane[7,8] or ethane[7,9], with current Density-Functional-Theory (DFT) calculations still exhibiting somehow large, uncontrolled inaccuracies of about 1 eV in the excess-electron ground-state energies. In addition, one-electron methods permits the simulation of much larger systems than DFT, allowing for a better description of strongly inhomogeneous systems such as interfaces.

In the context of organic alkane insulators, DFT calculations has been recently[8] benchmarked against experimental results of excess electrons in fluid methane. DFT methods, even using the hybrid B3LYP functional, were not able[8] to provide an accurate prediction for the excess electron ground-state energy, with large discrepancies with respect the experimental values, up to 2 or 3 eV. On the other hand, one-electron pseudopotential methods[7], based on fully ab initio calculations, have been shown to provide accurate predictions, with energy discrepancies smaller than 0.1 eV. A similar agreement is found in larger-chain alkane insulators such as ethane or propane[7,9]. While the success of the one-electron method can be physically justified in the strong Pauli repulsion between the excess electron and the electrons at the atoms in these insulators—with a fundamental band gap of about 9 eV— , the ultimate justification lies in the observed unrivaled agreement with experimental data.

In a recent work[10], the lowest excess-electron states on PE-vacuum interfaces were studied using DFT and the same one-electron pseudopotential considered here—also called a *Lanczos* method in Refs.[8,10]. Here we extend that study by considering larger samples of PE, which reveals previously unnoticed differences in the excess electron states at the amorphous and crystalline surfaces. Furthermore, the one-electron method used in Ref.[10] to account for the long-range interaction with the excess electron was based on a perturbation theory technique which, although providing a good estimation of the excess-electron energies, does not describe precisely the long-range interaction of the excess electron with the surface of the dielectric.

It is well known that an excess electron feels an attraction to the surface of a dielectric, forming surface states. From purely electrostatic considerations, using for example the method of mirror charges[11], a point charge near the surface of a dielectric (at, say $z = z_0$) feels a Coulomb, attractive interaction with the mirror charge at the dielectric ($z = -z_0$). This Coulomb electrostatic po-

[a] State Key Lab. of Electrical Insulation and Power Equipment, Xi'an Jiaotong University, No. 28 Xianning West Road, Xi'an 710049, Shaanxi, China.
[b] Departamento de Física Aplicada I, EUP, Universidad de Sevilla, Calle Virgen de África 7, 41011 Sevilla, Spain; E-mail: dcubero@us.es

† Electronic Supplementary Information (ESI) available: [with further details of the pseudopotential describing the interaction of the atoms with the excess electron]. See DOI: 10.1039/b000000x/

View Article Online
DOI: 10.1039/C8CP06897F

tential goes to minus infinity as the point charge approaches the dielectric surface ($z = 0$). However, a real excess electron would not feel a continuum medium at such a short distance, but a finite interaction with the nearest atoms at the dielectric. In this paper, we implement a reaction-field method that takes into account the discrete atomistic interaction at short distances, as well as the Coulomb long-range interaction with the dielectric interface at larger distances.

The paper is organized as follows. First, we present in Sec. 2 the reaction-field method we have developed to account for the long-range interaction with the interface, the simple perturbation theory method used in Ref.[10], and the simulation technique used to generate large samples of polyethylene/vacuum interfaces. In Sec. 3 we discuss the excess-electron surface states found in amorphous and crystalline interfaces of polyethylene, in addition to a comparison with the results reported in Ref.[10] for smaller slabs using the perturbation theory method. Finally, Sec. 4 ends with the main conclusions.

2 Methodology

2.1 A reaction-field method for the interface

The main idea behind the reaction-field method is that the atomic landscape surrounding the excess electron can be divided into two parts: i) inside a cutoff sphere, of radius R_c, centered at the point charge, in which the atoms are treated explicitly in a discrete manner; and ii) the region outside the cutoff sphere, in which the dielectric is regarded as a continuum medium, with a uniform and isotropic permitivity ε. The assumption is that the cutoff radius is large enough, so that the atoms are far away from the electron and their interaction can be described with a continuum model. The excess electron creates a polarization on the truncated dielectric medium —i.e. the whole dielectric without the cutoff sphere—, which in turn produces an electric field $\mathbf{E}_{\rm RF}$ that is felt by the excess electron and every atom inside the cutoff sphere.

The permitivity ε can be determined from experiment, or, more consistently, from a bulk simulation using the own force-field[9,12,13], which may use ab initio data for the atomic polarizabilities[9] —see more details in Sec. 2.2.

The reaction-field method is frequently used to describe dipole-dipole interactions[12] in homogeneous systems as a simple, fast alternative to Ewald sums. Even in highly inhomogeneous systems, like in vapor-liquid or solid-liquid interfaces, the application of a reaction-field method specifically designed for homogeneous systems can provide reasonable results[14]. However, the semi-continuum ideas behind the reaction-field technique are not limited to homogeneous systems. In this section we present a reaction-field method specifically designed for flat interfaces between two mediums with different permitivities.

Let us assume that at $z < 0$ there is a dielectric of permitivity ε, whereas at $z > 0$ the permitivity is ε_0. The system is infinite in the x and y directions. Thus, without loss of generality, we can assume the excess electron, with charge q, is located along the z-axis at $\mathbf{r}_0 = (0,0,z_0)$.

The electrostatic potential V_0 created by the point charge and

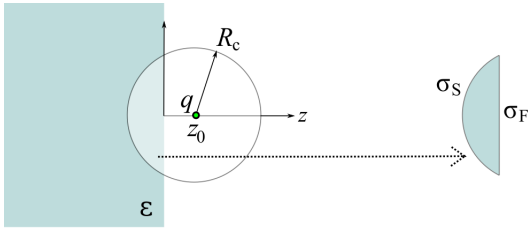

Fig. 1 Calculation of the reaction field. The dielectric, with permitivity ε, is at $z < 0$, the excess electron, with charge q, is at $z = z_0$, and the cutoff sphere, with radius R_c is centered at the point charge. The atoms inside the cutoff sphere are explicitly taken into account in the simulations, while the region in the dielectric, after subtracting the cutoff sphere part, is considered as a continuum dielectric, creating a reaction field $\mathbf{E}_{\rm RF}$ inside the sphere. This field is computed by subtracting the contribution created by the dielectric region inside the cutoff sphere, which is generated by the surface polarization densities σ_S and σ_F.

the full continuum dielectric can be easily computed at any point in space by using the method of mirror charges[11]. We are here interested in the (reaction-field) potential $V_{\rm RF}$ created by the remaining part of the dielectric after subtracting the dielectric region inside the cutoff sphere centered at the excess electron, i.e.

$$V_{\rm RF} = V_0 - \frac{q}{4\pi\varepsilon_0|\mathbf{r}-\mathbf{r}_0|} - V_S - V_F, \tag{1}$$

where $\mathbf{r} = (x,y,z)$, V_S is the potential created by the polarization surface charge density σ_S at the part of the cutoff sphere's surface inside the dielectric, and V_F the potential created by the polarization surface charge density σ_F at the dielectric's surface inside the cutoff sphere, see Fig. 1. As reported below, these surface densities can be computed from the analytical expression of V_0. In turn, given the expresions of V_0, σ_S and σ_F, the electric reaction field, $\mathbf{E}_{\rm RF} = -\nabla V_{\rm RF}$, can be easily computed at every atom inside the cutoff sphere, at each timestep of the simulation, by direct numerical integration. This is a necessary step in the self-consistent algorithm used in the simulations to compute the local field at each atom[9]. Furthermore, the simulation also requires the interaction energy $U_{\rm RF}$ between the excess electron and the remaining part of the dielectric (dielectric without the cutoff sphere part), i.e.

$$U_{\rm RF} = \frac{q}{2} V_{\rm RF}(\mathbf{r}_0). \tag{2}$$

2.1.1 Point charge at the vacuum.

For $z_0 > 0$, the full potential is given by[11]

$$V_0(\mathbf{r}) = \begin{cases} \frac{1}{4\pi\varepsilon_2}\left(\frac{q+q'}{|\mathbf{r}-\mathbf{r}_0|}\right) & z < 0 \\ \frac{1}{4\pi\varepsilon_0}\left(\frac{q}{|\mathbf{r}-\mathbf{r}_0|} + \frac{q'}{|\mathbf{r}+\mathbf{r}_0|}\right) & z > 0 \end{cases} \tag{3}$$

where

$$q' = -q\left(\frac{\varepsilon-\varepsilon_0}{\varepsilon+\varepsilon_0}\right). \tag{4}$$

The charge density at the dielectric surface, at a distance $\rho = \sqrt{x^2+y^2}$, is then given by ($\mathbf{E}_0 = -\nabla V_0$)

$$\sigma_F(\rho) = (\varepsilon-\varepsilon_0)\mathbf{E}_\mathbf{0}\cdot\mathbf{e}_z = \frac{q'}{2\pi}\frac{d}{(\rho^2+z_0^2)^{3/2}}, \tag{5}$$

View Article Online
DOI: 10.1039/C8CP06897F

and at the cutoff sphere surface

$$\sigma_S = (\varepsilon - \varepsilon_0)\mathbf{E_0}\cdot(\mathbf{r}-\mathbf{r}_0)/|\mathbf{r}-\mathbf{r}_0| = -\frac{q'}{2\pi R_c^2}, \tag{6}$$

which yields, after a somehow lengthy, but straightforward calculation,

$$U_{\mathrm{RF}} = \begin{cases} \frac{qq'}{8\pi\varepsilon_0 R_c}\left(1-\frac{z_0}{2R_c}\right) & 0 \le z_0 \le R_c \\ \frac{qq'}{16\pi\varepsilon_0 z_0} & R_c \le z_0 \end{cases} \tag{7}$$

Note that for $z_0 > R_c$ the reaction-field energy (7) explicitly accounts for the expected Coulomb interaction between the point charge and the dielectric surface.

2.1.2 Point charge at the dielectric.

For $z_0 < 0$, the full potential is [11]

$$V_0(\mathbf{r}) = \begin{cases} \frac{1}{4\pi\varepsilon_2}\left(\frac{q}{|\mathbf{r}-\mathbf{r_0}|}+\frac{-q'}{|\mathbf{r}+\mathbf{r}_0|}\right) & z<0 \\ \frac{1}{4\pi\varepsilon_0}\left(\frac{q+q'}{|\mathbf{r}-\mathbf{r_0}|}\right) & z>0 \end{cases} \tag{8}$$

which implies

$$\sigma_F(\rho) = \frac{-q'\varepsilon_0}{2\pi\varepsilon}\frac{d}{(\rho^2+z_0^2)^{3/2}}, \tag{9}$$

and, with θ being the azimuth ($\cos\theta = (z-z_0)/R$),

$$\sigma_S(\theta) = \frac{\varepsilon-\varepsilon_0}{4\pi\varepsilon}\left[\frac{q}{R_c^2}+\frac{-q'(R_c+2z_0\cos\theta)}{(R_c^2+4z_0^2+4z_0R_c\cos\theta)^{3/2}}\right], \tag{10}$$

yielding

$$U_{\mathrm{RF}} = \begin{cases} \frac{qq'}{8\pi\varepsilon_0 R_c}\left(1-\frac{z_0}{2R_c}\frac{\varepsilon_0}{\varepsilon}\right) & 0 \le |z_0| \le R_c \\ \frac{qq'}{16\pi\varepsilon z_0}+\frac{\varepsilon+\varepsilon_0}{\varepsilon}\frac{qq'}{8\pi\varepsilon_0 R_c} & R_c \le |z_0| \end{cases} \tag{11}$$

2.2 The simple perturbation theory method

2.2.1 Homogeneous systems.

We can use the result (11) to obtain the reaction-field energy for the homogeneous case, i.e. for a simulation at the bulk of the dielectric. By taking the limit $z_0 \to -\infty$ in (11), the interface is sent away, yielding

$$U_{\mathrm{RF}} = -\frac{\varepsilon-\varepsilon_0}{\varepsilon}\frac{q^2}{8\pi\varepsilon_0 R_c}. \tag{12}$$

This energy can be interpreted as the long-range correction that has to be added to a bulk simulation in which only the interaction with the atoms inside the cutoff sphere is considered. In Ref. [9], by using a mean field approach [15], the following expression was used

$$U_{\mathrm{RF}} = -\frac{f_L\alpha_0 n}{2\varepsilon_0}\frac{q^2}{4\pi\varepsilon_0 R_c}, \tag{13}$$

where α_0 is the molecular polarizability*, n is the corresponding atomic number density, and $f_L = [1+(2/3)\alpha_0 n/\varepsilon_0]^{-1}$ is the Lorentz local-field factor [15,16].

* Note that the molecular polarizability α_0 is related to the molecular polarizability volume α reported in Ref. [9] by the formula $\alpha_0 = \alpha 4\pi\varepsilon_0$, due to the change between SI and cgs units.

Combining (12) and (13) yields the well-known Clausius-Mossetti equation

$$\frac{\varepsilon/\varepsilon_0-1}{\varepsilon/\varepsilon_0+2} = \frac{\alpha_0 n}{3\varepsilon_0}, \tag{14}$$

which relates the dielectric constant to the atomic polarizabilities.

Alternatively, the fact that the cutoff sphere must be sufficiently large to offer a good microscopic description suggests the use of $1/R_c$ as a small parameter in a perturbation theory approach. This leads to a dependency in the energy correction of the form

$$U_{\mathrm{RF}} = -\frac{A}{R_c}, \tag{15}$$

where A is a constant that can be obtained from the simulation by linear fitting the data obtained at different cutoffs. In fact, this method has been shown to provide corrections in excellent agreement with the above result (13) in homogeneous, isotropic setups such as fluid and amorphous phases [9].

2.2.2 Inhomogeneous systems.

The perturbation theory method of Eq. (15) is not limited to homogeneous or isotropic systems, thus providing a simple simulation technique useful for more complex setups. In Ref. [10] this method was applied to study PE-vacuum interfaces using small slabs.

Note that this technique provides a simple constant correction to the excess-electron energies, without otherwise modifying the electron interaction potential. As a consequence, the excess-electron wavefunctions are the same as those returned by a simulation with interactions truncated by the cutoff sphere, and thus less accurate than those obtained with the reaction-field method described above—which, for example, does not neglect the long-range Coulomb interaction with the dielectric interface. We compare the results of both methods in Sec. 3.2.

2.3 Generation of the PE-vacuum interface

The generation of atomic configurations in the simulation representing a PE-vacuum interface can be a tricky task for amorphous PE due to the polymeric character of the material: The atomic chains must fold back at the interface in a reasonable way, without the unnatural chain-breaking that would result by simply truncating a simulation cell used for the bulk—with periodic boundary conditions.

The new amorphous-vacuum interfaces reported in this paper were generated following a procedure similar to the one used in Ref. [13] for amorphous-lamellae interfaces. A single lamellae block with a thickness of about 50 Å, made up of 10 PE chains with 552 CH_2 units, was replicated one time in the z direction. The atom coordinates in the first lamellae block was kept fixed at all times, while the second block was melted by being in contact with a thermostat that increased its temperature from 300 K to 500 K in a time interval of 3 ns, being kept at 500 K for another 3 ns in order to insure the melting of the second block, and then quenched by cooling to 300 K over 3 ns. Periodic boundary conditions in all directions and a barostat, holding the pressure at 1 atm, was used in the simulations. Finally, the first lamellae block is removed, leaving an amorphous slab with a measured density that

View Article Online
DOI: 10.1039/C8CP06897F

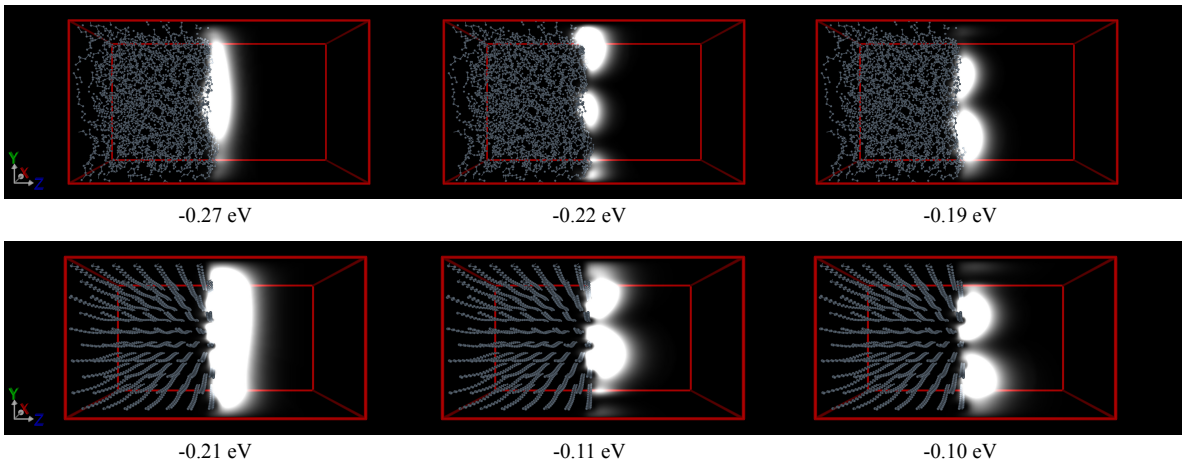

Fig. 2 Surface states at amorphous (top) and crystalline (bottom) polyethylene/vacuum interfaces. For each setup, the first three excess electron states are shown, with the numbers indicating the corresponding energies. The probability density of the excess electron at each point is represented as a source of light, the lighter the region the higher the probability density. The units CH_2 in the polymer chains are represented by a sphere.

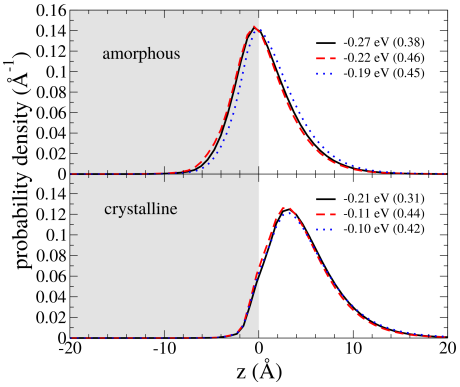

Fig. 3 Marginal probability density in the z-direction for the same states shown in Fig. 2. The numbers in brackets indicate the kinetic energy of each state (in eV).

is in good agreement with the experimental value[17] 0.86 g/cm^3.

The crystalline phases of PE were simulated with parallel all-trans PE chains which have their both ends connected through periodic boundary conditions along a direction perpendicular to the z-axis. The system was equilibrated at 300 K at constant pressure (1 atm), producing an atomic of density of 1.03 g/cm^3, also in agreement with the experimental measure[17] 1.01 g/cm^3.

Each slab provides two PE-vacuum interfaces, which were used in the simulation with the reaction-field method after transforming the z-coordinates in order to locate the interface of interest at $z = 0$. In these latter simulations, periodic boundary conditions were applied only in the x and y directions.

The force field and the rest of the technical details are like in Ref.[13], with a standard cutoff radius of $R_c = 9$ Å.

The rest of the details of the excess-electron pseudopotential are the same as in Ref.[9], which have been summarized for convenience in the Supplemental Material†.

The pseudopotential is computed on a 3D grid, with a fixed grid spacing of 0.7 Å, and the kinetic energy operator evaluated using a fast Fourier transform (FFT)—thus with a maximum energy of 76.7 eV from the grid spacing. The quantum states of the excess electron are then found by solving the Schrödinger equation using a standard Lanczos method[18].

3 Results and discussion

3.1 Amorphous and crystalline surface states

The application of the reaction-field method to the PE-vacuum interfaces produces the expected surface states, as shown in Fig. 2. Though all states are delocalized through a direction parallel to the interface, only the ground state is observed to extend somehow uniformly through the dielectric surface. The excited states show some points at the surface where the probability density is negligible, in analogy with the well-known nodes of one-dimensional eigenstates[19]—which exhibit an increasing number of nodes .

The shown excited levels also are observed to be quasidegenerated, an indication that they can be grouped[9] to form states with a finite momentum, moving along the dielectric surface.

Though the excess electron states at the amorphous and crystalline surfaces appear similar, they have some distinctive features. The amorphous surface exhibit deeper electron levels than the crystalline ones, about 0.06 eV deeper for the ground state and 0.1 eV for the following levels. Since averaging over 10 independently-generated configurations produces uncertainties in the observed levels of less than ± 0.01 eV, this distinct energy difference between both phases is not subject to thermostatistical fluctuations.

But the wave function exhibit larger discrepancies. Figure 3 shows the accumulated probability density in the direction perpendicular to the interface, clearly indicating that the excess electron sits at a distance from the crystalline surface, with a peak at about 3 Å from the dielectric—note the coordinate origin $z = 0$ is chosen to match the rightmost carbon in the PE slab. In contrast, the excess electron prefers to be nearer the amorphous surface, with the peak just inside the dielectric. These features are not particular of the ground state, as in each dielectric surface all levels are observed in Fig. 3 to collapse to almost the same marginal density—despite being distinctly different in the other directions,

View Article Online
DOI: 10.1039/C8CP06897F

as shown in Fig. 2.

The disparity between the surface states in the amorphous and crystalline interfaces can be rationalized by recalling the atomic density in each morphology and their effect on the excess electron. Inside the crystalline regions of PE the atomic density is known[13,20] to be very large for the excess electron, being the repulsion from the atomic centers the dominant interaction, and effectively expelling the electron out of the material. In Ref.[20] it was shown that this is mechanism was responsible for important differences in the excess-electron properties between the crystalline phases of PE and long-chain alkanes —which had been used as experimental models of PE—, with the excess electron residing at the empty gap separating the layers of long-chain alkanes.

In contrast, the atomic density in the amorphous region is much smaller, permitting the excess electron to lie closer to the atoms, and thus lowering its energy due to an increased polarization energy. This relationship between the electron energy values and atomic density has also been confirmed by the successful correspondence[13] between localized states and natural cavities—due to atomic density fluctuations—found in the bulk phases of PE.

The lowest energy levels in the PE-vacuum surfaces are inside the range of the localized states found[13] in the bulk of amorphous PE, which varies from -0.4 eV to -0.1 eV, though with the important difference that the surface states studied here are not localized, but extended throughout the dielectric surface. Their energies are also smaller than the energies of the conducting, extended states inside the amorphous and crystalline bulk regions, which are[13] larger than -0.1 eV and 0.46 eV, respectively.

3.2 Comparison with the perturbation theory method

Figure 4 shows the excess electron density for the first two surface levels, obtained with the perturbation theory method described in Sec. 2.2 for a typical PE-vacuum system studied in Ref.[10]. The PE slab is formed by 4 chains with 20 CH_2 units between a vacuum gap of almost 55 Å, with periodic boundary conditions being in place in all directions. The results obtained with the reaction-field method of Sec. 2.1, for this same configuration, are also plotted for comparison—two reaction-field simulations were run, one for each interface at each side of the slab.

First, note that the two shown levels of the perturbation theory method exhibit similar probability in both PE-vacuum interfaces. This feature is absent in the reaction-field method by construction, because in the latter case periodic boundary conditions are not considered in the direction perpendicular to the surface, and the reaction-field correction depends explicitly on the interface location and orientation. Since the surface states are intrinsically localized around a single interface, each level is doubled in the perturbation theory method—one state for each interface. This is confirmed by the quasi-degeneration shown in Fig. 4—a linear combination of both states can result in probability mainly in one interface.

However, note that, despite the large width (55 Å) of the vacuum region, finite size effects are still present in the perturbation theory calculation, as evidenced by the probability density of the lowest level in Fig. 4, which clearly does not decay to zero at the center of the vacuum gap—unlike the other states shown in the figure.

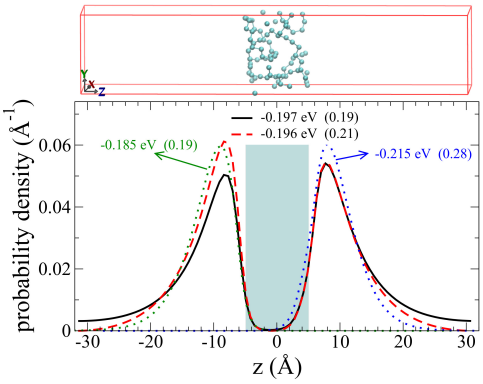

Fig. 4 Marginal probability density in the z-direction for a PE slab studied in Ref.[10] using the perturbation theory (black solid and red dashed line). The densities obtained with the reaction-field method are also shown (blue and green dotted lines), though they have been divided by 2 for the sake of the comparison. The numbers in brackets indicate the kinetic energy of each state. The top panel shows the atomic configuration in the simulation cell.

In fact, the comparison with the reaction-field method results indicates that the energy values obtained with the perturbation method are in reasonable agreement, but there are somehow larger discrepancies in the wave function—which, as discussed in Sec. 2.2.2, is expected given the nature of the perturbation theory method. While a reasonable agreement in the position of the distribution's peak can be seen in Fig. 4, and also in the tail that falls into the dielectric, the wave function's tail into the vacuum is not properly described by the perturbation theory method, distinctly showing a slower decay than the reaction-field method—both the ground and first excited state exhibit a slower decay, and thus also a linear combination of them. This is expected, since the perturbation theory method does not account for the Coulomb interaction of the excess electron with the dielectric surface—note, for example, that at a distance z_0 from the interface, with $z_0 > R_c$, there are no atoms inside the cutoff sphere and the simulation method consider no interaction with the excess electron. The reaction-field method, being specifically designed to include that interaction, is expected to provide a much better description of the wave function at the vacuum.

Let us notice that the surface states shown in Fig. 4 are more similar to the excess electron states at crystalline interfaces than amorphous interfaces, with the probability density peaking at the vacuum regions, at about 3 Å from the dielectric. This distance, together with the energy value, are in good agreement with the crystalline values shown in Fig. 3 These are also the same values that are obtained with the perturbation theory method in a lamellar PE-vacuum interface[10] in which the chains are perpendicular to the interface surface—ie. a crystalline slab with chain folds[13] at the interface. The fact that the same energies are obtained in crystalline surfaces, regardless of the orientation of the PE chains, validates the use of an isotropic permittivity in the reaction field method for crystalline setups.

View Article Online
DOI: 10.1039/C8CP06897F

The atomic configuration, shown at the top panel of Fig. 4, is not exactly crystalline, it does contains random chain folding and some degree of disorder. However, the real carbon-to-carbon density—defined from the leftmost carbon to the rightmost one—of that simulated slab is 1.1 g/cm^3, an atomic density actually larger than the accepted crystalline value 1.0 g/cm^3. As a reference, the carbon-to-carbon density of the amorphous slabs considered here is 0.86 g/cm^3—in good agreement with the experimental value. The high atomic density of the small slab shown in Fig. 4 causes the excess electron to locate itself well into the vacuum.

Therefore, the PE-vacuum interface studied in Fig. 4, despite being called amorphous in Ref.[10], produce surface states that are typical of crystalline, or highly packed regions. The same applies to the largest system considered in Ref.[10], a (supposedly amorphous) slab formed by 4 chains with 40 CH_2 units, which has a carbon-to-carbon density of 0.97 g/cm^3, also near the crystalline value, and thus producing equivalent results. This issue illustrates the perils of using slabs of limited size, a limitation that was in place in Ref.[10] due to the use of DFT methods on the same atomic configurations.

The energies predicted by DFT calculations[10] are off by about 1 eV when the hybrid functional B3LYP is used in a localized basis set, which was extended to include a lattice of ghost atoms. Since the excess electron is known to sit not near the atoms, but in the empty space between them, this extended basis set is needed to improve the predictions. However, a better description in the inter-atomic space is offered by a plane-wave basis set, and the best agreement in the excess-electron wave function is found[10] with the simpler functional LDA+BP using plane waves, showing a peak at about the same distance from the dielectric than the one predicted in this work. Unfortunately, the energy values obtained with this latter DFT method are off by several eV's in the bulk[10].

4 Conclusions

We have studied the excess electron states at polyethylene/vacuum interfaces using a one-electron pseudopotential method, which involves mixed quantum-classical simulations, with an accurate reaction-field method specifically designed to account for the Coulomb interaction of the excess electron with the dielectric surface. The reaction-field method is based on a partition of the region surrounding the electron into two zones: one inner region treated with atomistic detail, the further one regarded as a continuum dielectric. Explicit expressions are given in Sec. 2.1 for the interaction energy and for the calculation of the electric field created by the continuum region.

The use of a one-electron pseudopotential method permitted the simulation of large interfaces, showing distinct differences between amorphous and crystalline interfaces. Due to the smaller atomic density in amorphous surfaces, the excess electron is able to penetrate the dielectric more than in the crystalline ones, being the probability maximum just inside the dielectric in the former, and sitting at a distance of about 3 Å in the latter.

The comparison with recent results[10] using a perturbation theory method shows reasonable agreement with the excess electron energies, and with some features of the wave function, but not with the tail in the vacuum region, showing a much smaller decay than with the more accurate reaction-field method. This disagreement is expected, given than the perturbation theory method does not account for the long range, Coulomb interaction of the excess electron with the dielectric surface.

The simulation of large interfaces has allowed us to provide accurate results to amorphous PE surfaces, and, in consequence, to identify the disordered, small slabs studied in Ref.[10] as crystalline or lamellar-like, given the obtained energy values and wave function features. This identification is confirmed by the real atomic density of the simulated slabs in Ref.[10], which was typical of the crystal or lamellar phase.

The method described here can be easily extended to more complex situations, involving (planar) interfaces between different dielectrics, such as PE-water, or other materials.

Conflicts of interest

There are no conflicts to declare.

Acknowledgements

DC acknowledges financial support from the Ministerio de Economía y Competitividad of Spain, Grant No. FIS2016-80244-P, and YW support from the National Science Foundation of China, with Grant No. 51507125.

Notes and references

1 J. Bisquert, *The Physics of Solar Cells: Perovskites, Organics, and Photovoltaic Fundamentals*, CRC Press, Boca Raton, 2017.
2 L. A. Dissado and J. C. Fothergill, *Electrical Degradation and Breakdown in Polymers*, P. Peregrinus, London, 1992.
3 D. Cubero and T. Takada, in *Tailoring of Nanocomposite Dielectrics - From Fundamentals to Devices and Applications*, ed. T. Tanaka and A. Vaughan, Pan Stanford, 2016, ch. 7: Computer Simulation of Nanocomposites at the Molecular Level, pp. 195–218.
4 L. Turi, W. Sheu and P. Rossky, *Science*, 2005, **309**, 914–917.
5 R. Larsen, W. Glover and B. Schwartz, *Science*, 2010, **329**, 65–69.
6 L. Turi and P. Rossky, *Chem. Rev.*, 2012, **112**, 5641–5674.
7 Z. Liu and B. J. Berne, *J. Chem. Phys.*, 1993, **99**, 9054–9069.
8 F. Saiz, N. Quirke, L. Bernasconi and D. Cubero, *Chem. Phys. Lett.*, 2016, **664**, 143–148.
9 D. Cubero, N. Quirke and D. F. Coker, *J. Chem. Phys.*, 2003, **119**, 2669–2679.
10 F. Saiz, D. Cubero and N. Quirke, *Phys. Chem. Chem. Phys.*, 2018, **20**, 25186–25194.
11 J. Jackson, *Classical Electrodynamics*, 3rd ed. Wiley, New York, 1999.
12 M. Allen and D. Tildesley, *Computer simulation of liquids*, Oxford Science Publications, Oxford, 1997.
13 Y. Wang, D. MacKernan, D. Cubero, D. Coker and N. Quirke, *J. Chem. Phys.*, 2014, **140**, 154902.
14 J. M. Miguez, D. Gonzalez-Salgado, J. Legido and M. M. P. neiro, *J. Chem. Phys.*, 2010, **132**, 184102.
15 J. Lekner, *Phys. Rev.*, 1967, **158**, 130.

View Article Online
DOI: 10.1039/C8CP06897F

16 D. Cubero and N. Quirke, *J. Chem. Phys.*, 2004, **120**, 7772–7778.

17 J. Brandrup and E. H. Immergut, *Polymer Handbook*, American Institute of Physics, New York, 1989.

18 L. Komzsik, *The Lanczos method : evolution and application*, Siam, Philadelphia, 2003.

19 E. Merzbacher, *Quantum Mechanics*, 3rd ed. Wiley, New York, 1998.

20 D. Cubero, N. Quirke and D. F. Coker, *Chem. Phys. Lett.*, 2003, **370**, 21–25.